

# Morphological, Structural, and Compositional Evolution of Pt–Ni Octahedral Electrocatalysts with Pt-Rich Edges and Ni-Rich Core: Toward the Rational Design of Electrocatalysts for the Oxygen Reduction Reaction

Meital Shviro,\* Martin Gocyla, Shlomi Polani, Marc Heggen, David Zitoun, and Rafal E. Dunin-Borkowski

The progress in colloidal synthesis of Pt–Ni octahedra has been instrumental in rising the oxygen reduction reaction catalytic activity high above the benchmark of Pt catalysts. This impressive catalytic performance is believed to result from the exposure of the most active catalytic sites after an activation process, chemical or electrochemical, which leads to a Pt surface enrichment. A foremost importance is to understand the structure and the elemental distribution of Pt–Ni octahedral, which leads to an optimal catalytic activity and stability. However, the factors governing the synthesis of the Pt–Ni octahedra are not well understood. In this study, unprecedented surface atomic segregation of Pt atoms in a Ni-rich Pt–Ni octahedral nanoparticle structure is established by advanced electron microscopy. The Pt atoms are almost exclusively located on the edges of the Pt–Ni octahedra. This structure is formed in a pristine form, i.e., prior to any chemical or electrochemical etching. A new growth mechanism is revealed, which involves the transformation from an octahedron with a Pt-rich core to a Ni-rich octahedron with Pt-rich edges. This observation may pave the way for a deeper understanding of this class of Pt–Ni octahedral nanoparticles as an electrocatalyst.

## 1. Introduction

The progresses of electrocatalysis on modeled surfaces have been impressive, reaching unprecedented levels of activity for platinum based alloys.<sup>[1]</sup> In recent years, the colloidal chemistry has followed the path opened on these low precious group metal (PGM) systems with deep control on the composition and shape of the low PGM nanocatalysts. As a result of the discovery of the extraordinary activity on extended Pt<sub>3</sub>Ni surfaces,

the advances in the preparation of binary alloy Pt–Ni nanoparticles (NPs) with controlled size,<sup>[2]</sup> shape,<sup>[3,4]</sup> and support<sup>[5,6]</sup> have driven a considerable interest for the synthesis of Pt–Ni octahedra as oxygen reduction reaction (ORR) electrocatalysts in proton exchange membrane fuel cells (PEMFCs).<sup>[7]</sup> Beside in PEMFCs, Pt–Ni based materials are, e.g., used as electrocatalysts for the methanol electrooxidation in direct methanol fuel cells.<sup>[8]</sup> However, binary Pt<sub>3</sub>Ni-alloy octahedra exhibit the highest performances reported so far as ORR electrocatalysts.<sup>[9]</sup> Different annealing treatments on Pt–Ni NPs<sup>[10,11]</sup> as well as the addition of a third transition metal,<sup>[12,13]</sup> on top of the Pt<sub>3</sub>Ni composition has led to the report of unprecedented ORR activity and durability. In most of the reports, the octahedral nanocrystals are Pt<sub>3</sub>Ni alloys and the third transition metal is located mainly on the surface.<sup>[12,14–16]</sup>


Ni-rich Pt alloys have scarcely been investigated since these compositions should not be stable in acidic medium, although enriched Pt surfaces or dealloyed systems can provide highly active and stable catalysts.<sup>[17–19]</sup> When changing the pH value to alkaline conditions, Ni-based nanostructures can be considered as valuable catalysts for the ORR.<sup>[20,21]</sup> However, for Ni-rich Pt–Ni octahedra a previous study shows a nanoscale phase segregation of a Pt-rich skeleton with a Pt-rich core.<sup>[22]</sup> The presence of a very strong ligand ( $\sigma$ -donor and  $\pi$ -acceptor) is instrumental to drive the compositional segregation.

Despite the achievements reported above, the relatively low level of understanding on the mechanism at work during the synthesis could impede further rational design of the synthetic pathway. As a matter of fact, only few studies demonstrate a direct correlation between the compositional structure of the Pt–Ni octahedra before and after electrochemical etching.<sup>[13,18,23]</sup>

In this study, advanced electron microscopy brings direct evidences for the surface atomic segregation of Pt atoms in Ni-rich Pt–Ni octahedra already in the pristine samples, without any chemical or electrochemical treatment, by using soft coordination ligands. The Pt atoms are almost exclusively located on the edges of the Pt–Ni octahedra. For this octahedral structure, the

Dr. M. Shviro, M. Gocyla, Dr. M. Heggen, Prof. R. E. Dunin-Borkowski  
Ernst-Ruska Centre for Microscopy and Spectroscopy  
with Electrons and Peter Grünberg Institute  
Forschungszentrum Jülich GmbH, 52425 Jülich, Germany  
E-mail: m.shviro@fz-juelich.de

S. Polani, Prof. D. Zitoun  
Department of Chemistry  
Bar Ilan Institute of Nanotechnology and Advanced Materials (BINA)  
Ramat Gan 52900, Israel

 The ORCID identification number(s) for the author(s) of this article can be found under <https://doi.org/10.1002/ppsc.201800442>.

DOI: 10.1002/ppsc.201800442

growth mechanism is studied. To the best of our knowledge, the observed level of atomic segregation without the presence of a Pt-rich core in Pt–Ni octahedral NPs was not yet reported.

## 2. Results and Discussion

Uniform Pt–Ni octahedral nanocrystals have been synthesized, following a surfactant-assisted wet process. The origin method<sup>[3]</sup> has been slightly modified to yield larger batches. Briefly, the nanocrystals have been synthesized in benzyl alcohol (BA) in the presence of polyvinylpyrrolidone (PVP) and benzoic acid. The surfactants used are soft ligands (carboxylic acid and pyrrolidone) and interact weakly with the metallic surface, contrary to the synthetic pathways involving a CO source (mainly  $W(CO)_6$ ). **Figure 1** shows high angle annular dark field (HAADF) scanning transmission electron microscopy (STEM) images which provide an image contrast depending on the atomic number (Z-contrast). The Z-contrast images suggest a nonuniform distribution of Pt and Ni within the nanocrystals. The NPs have an octahedral shape with regular size of  $14.1 \pm 1.6$  nm (vertex to vertex along the  $\langle 100 \rangle$  direction). The fast Fourier transform (FFT) applied to the high resolution (HR) HAADF-STEM image of the Pt–Ni octahedra in **Figure 1b** shows a face-centered cubic (FCC) phase with a lattice parameter of 0.36 nm (close to FCC Ni: 0.354 nm).

**Figure 2a** shows a HR HAADF-STEM image of an octahedron close to the  $\langle 100 \rangle$  zone axis. Diagonal bright lines on a darker background are clearly visible. In addition, a bright strip is visible at the edge of the octahedron (the arrow in **Figure 2a** is a guide for the eye), i.e., in a part which is thinner than the dark facet regions. The bright contrast features coincide with the location of the edges of the octahedron in **Figure 2** as well as in **Figure 1**, which indicates the presence of Ni-rich octahedral with Pt-rich edges.

To underline the HAADF-STEM results, additional energy dispersive X-ray (EDX) measurements were carried on. **Figure 2b** presents the Pt and Ni distribution in the octahedron in **Figure 2a** and supports the structural description above:

The bright lines in **Figure 2a** coincide with the distribution of Pt in the EDX map in **Figure 2c**. Additionally, the Ni EDX map in **Figure 2d** shows a continuous Ni distribution. The atomic composition of Pt–Ni has been set to  $Pt_{17}Ni_{83}$  by the initial stoichiometry of metal acetylacetonate precursors, which is confirmed by inductively coupled plasma atomic emission spectroscopy (ICP-AES) analysis: The composition of the NP measured by EDX and imaged in **Figure 2a** is Pt 12 at% and Ni 88 at%.

Different synthetic pathways lead to octahedral structures with different segregation and Pt content. Gan et al.<sup>[24]</sup> reported on a synthetic pathway where Pt-rich seeds evolve in a Pt-rich hexapod and finally Ni filled the facets to form octahedra. Oh et al.<sup>[22]</sup> showed a segregated structure of Pt-rich hexapod along with Pt-rich edges. Chang et al.<sup>[23]</sup> investigated octahedra with Pt-rich core and Pt–Ni alloy surrounding. And, we<sup>[25]</sup> recently reported on octahedra with Pt-rich shell and Ni-rich core.

Previous work<sup>[26]</sup> demonstrated the simulation of 2D ADF-STEM images and EDX maps for different 3D Pt–Ni octahedral structures. To correlate the 2D HAADF-STEM image and the EDX map in this study (**Figure 2**) with the four known 3D octahedral structures from literature the following octahedral structure types should be considered: 1) a “Pt hexapod” octahedral structure where the octahedral structure consisting of a Pt-rich hexapod oriented along crystallographic  $\langle 100 \rangle$  directions and a Ni-rich region at the  $\{111\}$  faces, 2) a “Pt core, Pt hexapod, and Pt edges” octahedral structure where an octahedral structure is like in (1) but with a Pt sphere in the core and a Pt decoration on the edges of the NP, 3) a “Pt–Ni alloy” octahedral structure where an octahedral structure consisting of a random mixture of Pt and Ni, and 4) a “Pt shell and Ni core” octahedral structure.

- 1) An octahedral structure imaged along the  $\langle 100 \rangle$  zone axis containing a Pt hexapod would lead to a representative 2D HAADF-STEM image with two bright diagonals but without a brighter area at the outer edges of the octahedra. In the corresponding Pt EDX map, Pt-rich diagonals would be seen and a lack of Ni signal in the area of the Pt-rich diagonals for the

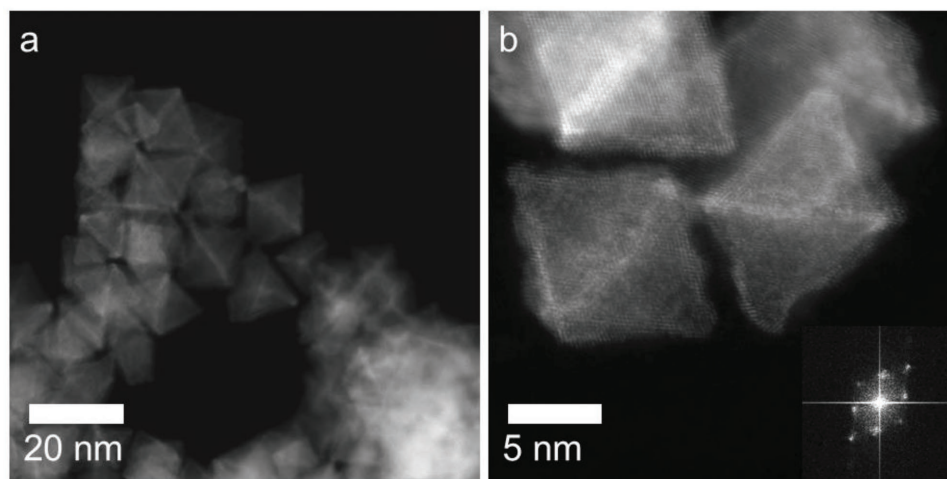


**Figure 1.** a) Overview HAADF STEM image of Pt–Ni octahedra and b) HR HAADF-STEM image with inset showing the corresponding FFT pattern in the bottom right.

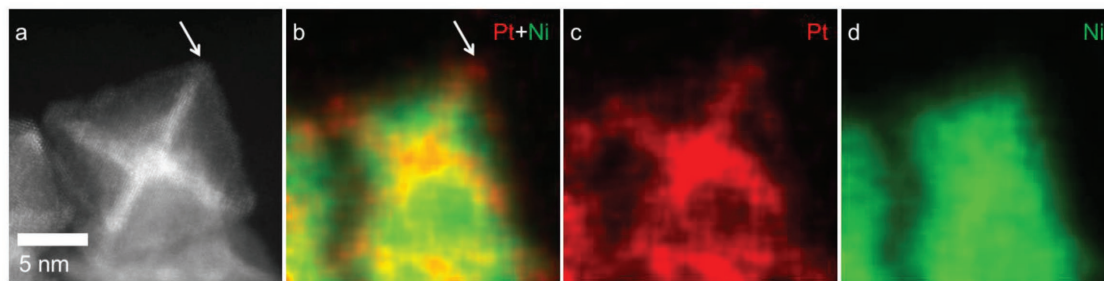


**Figure 2.** a) HR HAADF-STEM image of Pt–Ni octahedra. b,c,d) Distribution of Pt (red) and Ni (green) in EDX composition maps. Arrows in (a) and (b) mark Pt-rich edges.

Ni EDX map. Thus, the nanocrystals presented in Figure 2a are clearly different from the “Pt hexapod” structure.

- 2) An octahedron with “Pt core, Pt hexapod, and Pt edges” oriented close to the  $\langle 100 \rangle$  zone axis would show two bright diagonals and bright outer edges for the HAADF-STEM image and a Pt-rich stripe in the Pt EDX map. However, the lack of Ni signal especially in the center of the nanocrystal differentiates this structure from the continuous distribution of Ni observed in Figure 2.
- 3) A “Pt–Ni alloy” octahedral structure oriented close to the  $\langle 100 \rangle$  zone axis would show a continuous Ni and Pt distribution in the EDX maps, i.e., the absence of diagonal stripes in HAADF-STEM image as well as in the Pt EDX maps. Hence, a Pt–Ni alloy octahedron is again different from that one presented in Figure 2.
- 4) Finally, a “Pt shell and Ni core” octahedral structure oriented close to the  $\langle 100 \rangle$  zone axis would show a continuous Ni distribution in the center, while a Pt-rich stripe would appear at the outer part of the octahedra in both the HAADF-STEM and the EDX maps. However, an absence of diagonal stripes in HAADF-STEM image as well as in the Pt EDX maps would differentiate this structure like for (3).

Considering a 3D octahedral structure with a Ni core and Pt edges would lead to 2D representatives, which fulfill all characteristics of Figure 2 with diagonal stripes and a thin stripe at the outer part of the octahedra both in HAADF-STEM image and Pt EDX map as well as continues Ni signal in the Ni EDX map.

Most reported synthetic pathways<sup>[22–24]</sup> yield octahedra with Pt-rich cores, while Pt–Ni octahedra display a very strong Pt

enrichment of outer parts of the octahedra are rare.<sup>[25]</sup> In our case, the Pt atoms are almost exclusively located on the edges of the Pt–Ni octahedra, while the Ni atoms form the core and the facets of the octahedra. As mentioned above the ratio of Ni to Pt has been set to 4.8 which corresponds, according to the bulk phase diagram of the binary compounds, to a solid solution and a statistical alloy of the two metals. Indeed, Wu et al.<sup>[3]</sup> conclude for the original synthesis an even distribution of Pt and Ni inside the octahedra. This conclusion is however based on overview HAADF-STEM images and elemental maps. The potential presence of Pt segregation at the edges of the octahedra cannot be seen clearly in a medium-resolution overview HAADF-STEM image or in an overview EDX map like the ones presented.<sup>[3]</sup> Our work also shows that medium-resolution overview HAADF-STEM images are insufficient to observe such details and HR HAADF-STEM images and HR EDX maps are required. Wu et al.<sup>[3]</sup> original synthesis shows octahedra with nonuniform Pt and Ni distribution (Figure S1, Supporting Information). As described above, our study presents direct evidence for a different Pt and Ni distribution for this synthesis compared to Wu et al.<sup>[3]</sup> original synthesis.

The detailed formation process of octahedra with Pt-rich edges and Ni-rich core was studied by analyzing HAADF-STEM images at intermediate reaction stages (Figure 3). At the initial stage after 10 min reaction time the Z-contrast image in Figure 3a shows an irregular NP with a bright core and a dark shell indicating the formation of a Pt core and Ni shell NP due to the faster decomposition of the Pt precursor and the reduction kinetics compared to the Ni precursor. Predicted trends of core–shell preferences between atoms from different groups show that the element with the larger cohesive energy, here Pt,

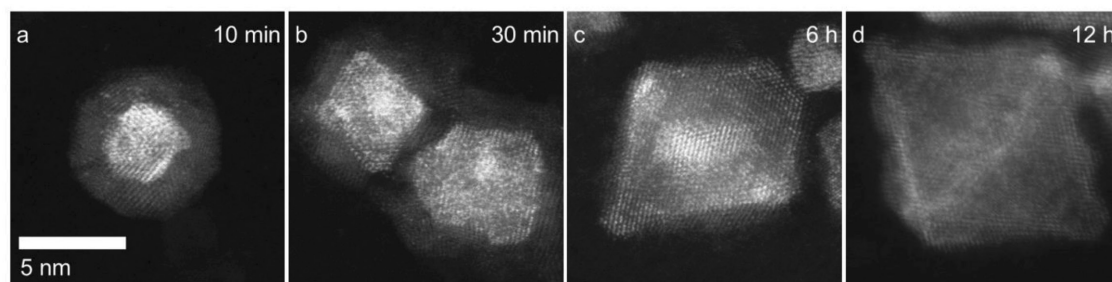


**Figure 3.** Growth study of Pt–Ni octahedra. a–d) HAADF-STEM images of Pt–Ni nanocrystals after a reaction time of a) 10 min, b) 30 min, c) 6 h, and d) 12 h.

goes to the core.<sup>[27]</sup> After 30 min reaction time, partly octahedral and partly irregular NPs with a small strong bright core, a bright surrounding and a thin less bright shell in the HAADF-STEM image (Figure 3b) are observed. This observation suggests a migration of Ni atoms into the core and the movement of Pt toward the surface, building a nanoparticle with Pt core, Pt–Ni alloy area, and a thin Ni shell. As reported on clusters, the large radius atoms of the minor component (here Pt) of an alloy have a tendency to migrate to the surface for geometrical reasons and might explain our observation and was the focus in recent studies.<sup>[22,28–30]</sup> When extending the reaction time to 3–6 h, octahedral NPs are found with a bright core and  $\langle 110 \rangle$  edges in the HAADF-STEM image in Figure 3c indicating the presence of a Ni-rich octahedron with a Pt core, and Pt edges.

This octahedral NP structure is similar to the octahedral described by Oh et al.<sup>[22]</sup> They also presented a very similar model for their structural evolution: The Pt atoms in the core diffuse to the  $\langle 110 \rangle$  edges facilitated by CO chemisorption and forming the octahedral structure with Pt core and Pt-rich edges.<sup>[22]</sup> By using density functional theory (DFT) calculations they showed that the strain leads to the segregation of Pt.<sup>[22]</sup> In the same study,<sup>[22]</sup> an octahedral structure with a Pt core and Pt-rich edges is the final product, while, in the present work a different final octahedral structure is found. Ultimately, after 12 h, octahedra with bright edges and an otherwise dark contrast distribution are found by HAADF-STEM imaging (Figure 3d), which is interpreted as a Ni-rich octahedra with Pt-rich edges

(Figure 2). The composition of the NPs measured by EDX during the structural evolution is in a range of Pt 6–14 at% and Ni 94–86 at%, which demonstrates the complete reaction of Pt from the early stage of the reaction. These results suggest the diffusion of Pt atoms as origin of the Pt-rich edges rather than a late Pt reduction or a site-selective Pt growth. Oh et al.<sup>[22]</sup> also attempted to obtain the final octahedral structure we present in our study, however CO was not sufficient enough to transfer all Pt atoms from the core to the  $\langle 110 \rangle$  edges.

In the following, we studied the role of each reagent in our synthesis on the resulting Ni core Pt edges octahedral structure to identify the key parameter to transfer all Pt atoms from the core to the  $\langle 110 \rangle$  edges.

As first step the effect of PVP and benzoic acid on both metal precursors were investigated. When only BA is used in the absence of both metal precursors, alloyed Pt–Ni nanoparticles with not well-defined shapes are formed with a composition of Pt 75 at% and Ni 25 at% (Figure 4b). With the addition of benzoic acid, Pt-rich cuboctahedra are formed with a uniform distribution of Pt and Ni forming an alloy (Figure 4f). The composition of the cuboctahedron is Pt 85 at% and Ni 15 at%, indicating a slower reduction rate of Ni. In the presence of PVP irregular shaped NPs are formed (Figure 4i), however a compositional segregation with a Pt-rich core, Ni-rich shell, and Pt-rich edges is visible (Figure 4j). The composition of this NP is Pt 6 at% and Ni 94 at%. Benzoic acid is needed for the formation of nanoparticles with well-defined shapes but the faster

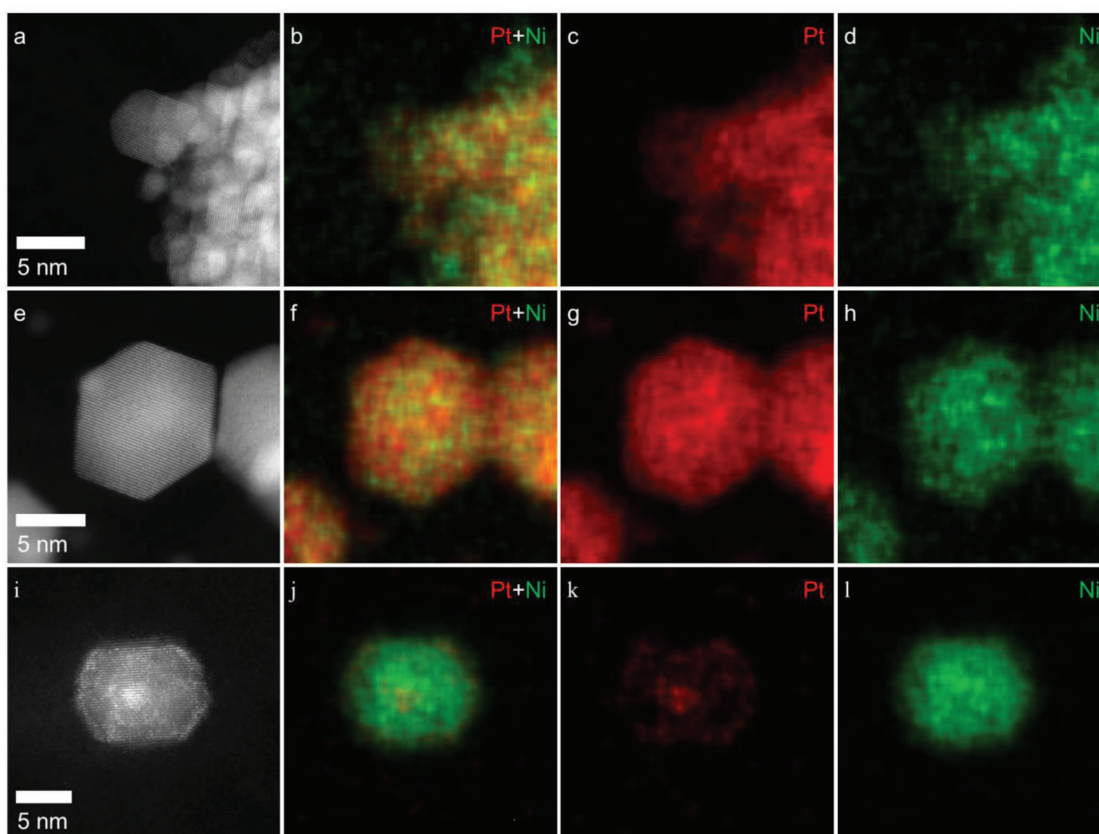


**Figure 4.** a,e,i) HR HAADF-STEM images and b–d,f–h,j–l) distribution of Pt (red) and Ni (green) in EDX composition maps for nanoparticles obtained without using a–d) PVP and benzoic acid, e–h) benzoic acid, and i–l) PVP.

reduction of Ni and the segregated structure in the absence of benzoic acid together with the slower reduction of Ni in the presence of benzoic acid indicate a dominant role of PVP on the reduction kinetics of Pt versus Ni for a segregation like in our octahedra with Ni-rich core and Pt-rich edges. This shows that PVP is the key compound to transfer all Pt atoms to the surface under our experimental conditions.

Further, we studied the role of the Ni precursor. In the presence of the solvent BA and Ni(acac)<sub>2</sub> no NPs were observed (Figure S2c, Supporting Information), indicating that BA alone is too weak to reduce Ni(acac)<sub>2</sub> at 150 °C. The addition of benzoic acid to BA and Ni(acac)<sub>2</sub> leads to the formation of NPs with spherical shapes (Figure S2f, Supporting Information) indicating that benzoic acid can act not only as surfactant but could be also important for the reduction of the Ni precursor. The addition of PVP to BA and Ni(acac)<sub>2</sub> leads to NPs with cuboctahedral shape (Figure S2i, Supporting Information), indicating that both compounds act not only as surfactants but are also important for the reduction of the Ni precursor. It is well established that capping agents binding to {111} facets direct the growth to octahedral shaped NPs and capping agents binding to {100} facets direct the growth to cuboctahedral NPs and finally to cubes due to changes in surface free energy and thereby different growth rates.<sup>[31]</sup> Therefore, the role of PVP in this synthetic environment might be acting as capping agent binding to {100} facets. Indeed, a computational study shows the stronger binding of PVP on the {100} facets of Ag<sup>[32]</sup> and supports our observation. Ni NPs with octahedral shape are formed in the presence of BA, Ni(acac)<sub>2</sub>, PVP, and benzoic acid (Figure S2l, Supporting Information), indicating that benzoic acid is acting in this environment as capping agent for the {111} surfaces. A stronger binding of the benzoic acid to the {111} facets compared to the binding of PVP to the {100} facets might increase the growth rate in <100> direction and the formation of Ni octahedral NPs. We have shown that Ni octahedra are formed even in the absence of a Pt precursor.

Next, the role of Pt(acac)<sub>2</sub> was studied. In the presence of BA and Pt(acac)<sub>2</sub>, spherical Pt nanoparticles are formed (Figure S3c, Supporting Information). While adding benzoic acid, irregular shaped Pt NPs are formed (Figure S3f, Supporting Information). Also while using PVP, BA, and Pt(acac)<sub>2</sub>, the formation of irregular shaped Pt NPs is visible (Figure S3i, Supporting Information). While both capping agents, PVP and benzoic acid, are

used in the presence of Pt(acac)<sub>2</sub>, mostly spherical nanoparticles but occasionally cuboctahedral nanostructures are found (Figure S3l, Supporting Information), underlining that the Ni precursor is needed for the formation of octahedra. The Ni precursor might strengthen the binding of the benzoic acid to the {111} facets and thus increase the growth rate in <100> direction to form the Pt–Ni octahedra.

Our above observations regarding the growth of the presented Ni-rich octahedral NP structure with Pt-rich edges are summarized in the illustration in **Figure 5** where we propose a morphological evolution sequence. The morphological evolution sequence starts with initially irregular Pt-core/Ni-shell NPs (Figure 5a). Upon longer reaction time, Pt gradually diffuses from the core toward the surface building Pt core, intermediate Pt–Ni alloy region, and Ni shell NPs (Figure 5b). Further reaction time leads to the formation of Ni-rich octahedral nanostructures with Pt-rich core and Pt-rich edges (Figure 5c) before finally Ni-rich octahedra with Pt-rich edges are found (Figure 5d).

Pt(acac)<sub>2</sub> facilitates the reduction of Ni(acac)<sub>2</sub> and/or the Ni-PVP complex, an interplay of BA, Ni, PVP and benzoic acid is needed to form the octahedral shape but PVP is the key component to transfer all Pt atoms from the core to the surface, to form this unusual segregated octahedra.

To the best of our knowledge, the segregation in the octahedra reported here, has not been reported for Pt–Ni octahedra, yet.

### 3. Conclusion

We synthesized a Pt–Ni octahedral NP electrocatalyst and found a previously unreported elemental segregation by HAADF-STEM, where Pt is located at the edges of Ni-rich octahedra. The growth mechanisms involve the subsequent formation of irregular shaped Pt-core/Ni-shell NPs, octahedral NPs with Pt-rich core and edges, and finally the transformation to Ni-rich octahedral NPs with Pt-rich edges. While the interplay between BA, Ni, PVP, and benzoic acid was shown to be the origin for the octahedral shape, PVP itself plays the dominant role for the Pt and Ni segregation acting as key component to transfer all Pt atoms from the core to the edges. Our discovered Pt–Ni octahedral NPs might be used as electrocatalyst with low

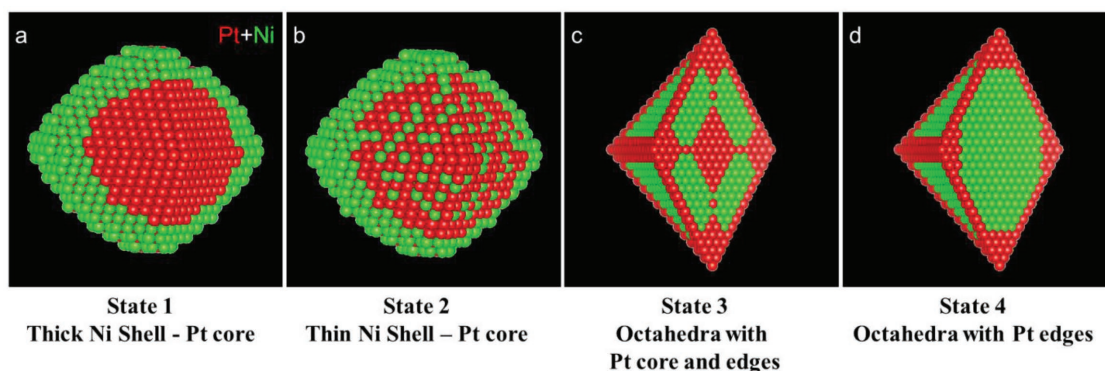


**Figure 5.** a–d) Illustrations of proposed Pt (red) and Ni (green) distributions in Pt–Ni octahedral nanocrystals that undergo transformations during synthesis.

Pt-content and thus our microstructural study on their structure and formation may facilitate a deeper understanding and tuning of their catalytic performance.

#### 4. Experimental Section

**Materials:** BA and benzoic acid (99.5% ACS) were purchased from Sigma-Aldrich. Platinum(II)acetylacetonate (Pt(acac)<sub>2</sub> (Pt 48% min), Nickel(II)acetylacetonate (Ni(acac)<sub>2</sub>, 95%), PVP (MW = 8000), and toluene (ACS, 99.5% min) were purchased from Alfa Aesar and Ethanol (96% min) was purchased from eal. Acetone (technical grade) was purchased from VWR chemicals. All materials were used as received.

**Synthesis of Pt–Ni Octahedral Nanoparticles:** Pt–Ni nanoparticles were synthesized using a route based on previous work.<sup>[33]</sup> Pt(acac)<sub>2</sub> (0.2 mmol), Ni(acac)<sub>2</sub> (0.93 mmol), PVP (0.0163 g), and benzoic acid (0.097 g) were dissolved in 10 mL of BA with 30 min vigorous stirring and transferred into a flask. The flask was heated to 150 °C for 12 h before being cooled naturally to room temperature. Pt–Ni nanoparticles were precipitated by acetone, separated via centrifugation, and purified by an ethanol–acetone mixture. For the control experiments, the respective compound/compounds were excluded, while all other parameters were kept constant.

**Morphological, Structural, and Elemental Characterization:** Transmission electron microscopy (TEM) images were done on an FEI (Thermo Fisher Scientific) Titan 80–300 electron microscope<sup>[34]</sup> equipped with a spherical aberration (C<sub>s</sub>) corrector (CEOS) for the objective lens. Experiments were carried out at 300 kV using the negative-C<sub>s</sub> imaging technique, which provides images with high contrast and low noise. STEM and EDX spectroscopy experiments were performed in an FEI (Thermo Fisher Scientific) Titan 80–300 electron microscope equipped with a probe corrector (CEOS) and an HAADF detector.<sup>[35]</sup> “Z-contrast” conditions were achieved by using a probe semiangle of 25 mrad and an inner collection angle of the detector of 68 mrad. For EDX elemental mapping, Pt L and Ni K peaks were used.

#### Supporting Information

Supporting Information is available from the Wiley Online Library or from the author.

#### Acknowledgements

Financial support was provided by the Deutsche Forschungsgemeinschaft (DFG) Grant No. HE 7192/1-1. M.S. acknowledges the Alexander von Humboldt Foundation and thanks the ESTEEM2 for financial support. M.S. and M.G. initiated the idea for this paper, designed the experiments, synthesized the material for control experiments, performed the HAADF-STEM experiments, processed the experimental data, interpreted the data and drafted the manuscript in Ernst-Ruska Centre for Microscopy and Spectroscopy with Electrons and Peter Grünberg Institute. S.P. synthesized the Pt–Ni octahedra in Bar Ilan Institute of Nanotechnology and Advanced Materials (BINA). All of the authors participated in scientific discussions and wrote the manuscript.

#### Conflict of Interest

The authors declare no conflict of interest.

#### Keywords

nanoparticles, phase segregation, Pt–Ni octahedra, structural evolution

Received: October 23, 2018

Revised: December 4, 2018

Published online:

- [1] P. Strasser, *Science* **2015**, *349*, 379.
- [2] Y. Yu, W. Yang, X. Sun, W. Zhu, X.-Z. Li, D. J. Sellmyer, S. Sun, *Nano Lett.* **2014**, *14*, 2778.
- [3] Y. Wu, S. Cai, D. Wang, W. He, Y. Li, *J. Am. Chem. Soc.* **2012**, *134*, 8975.
- [4] J. Zhang, H. Yang, J. Fang, S. Zou, *Nano Lett.* **2010**, *10*, 638.
- [5] C. Cui, L. Gan, M. Neumann, M. Heggen, B. R. Cuenya, P. Strasser, *J. Am. Chem. Soc.* **2014**, *136*, 4813.
- [6] C. Zhang, S. Y. Hwang, A. Trout, Z. Peng, *J. Am. Chem. Soc.* **2014**, *136*, 7805.
- [7] X. Zhou, Y. Gan, J. Du, D. Tian, R. Zhang, C. Yang, Z. Dai, *J. Power Sources* **2013**, *232*, 310.
- [8] L.-X. Ding, A.-L. Wang, G.-R. Li, Z.-Q. Liu, W.-X. Zhao, C.-Y. Su, Y.-X. Tong, *J. Am. Chem. Soc.* **2012**, *134*, 5730.
- [9] X. Wang, S.-I. Choi, L. T. Røling, M. Luo, C. Ma, L. Zhang, M. Chi, J. Liu, Z. Xie, J. A. Herron, M. Mavrikakis, Y. Xia, *Nat. Commun.* **2015**, *6*, 7594.
- [10] V. Beermann, M. Gocyla, S. Kühn, E. Padgett, H. Schmies, M. Goerlin, N. Erini, M. Shviro, M. Heggen, R. E. Dunin-Borkowski, D. A. Muller, P. Strasser, *J. Am. Chem. Soc.* **2017**, *139*, 16536.
- [11] M. Gocyla, S. Kuehl, M. Shviro, H. Heyen, S. Selve, R. E. Dunin-Borkowski, M. Heggen, P. Strasser, *ACS Nano* **2018**, *12*, 5306.
- [12] X. Huang, Z. Zhao, L. Cao, Y. Chen, E. Zhu, Z. Lin, M. Li, A. Yan, A. Zettl, Y. M. Wang, X. Duan, T. Mueller, Y. Huang, *Science* **2015**, *348*, 1230.
- [13] V. Beermann, M. Gocyla, E. Willinger, S. Rudi, M. Heggen, R. E. Dunin-Borkowski, M. G. Willinger, P. Strasser, *Nano Lett.* **2016**, *16*, 1719.
- [14] Q. Jia, Z. Zhao, L. Cao, J. Li, S. Ghoshal, V. Davies, E. Stavitski, K. Attenkofer, Z. Liu, M. Li, X. Duan, S. Mukerjee, T. Mueller, Y. Huang, *Nano Lett.* **2018**, *18*, 798.
- [15] L. Cao, T. Mueller, *Nano Lett.* **2016**, *16*, 7748.
- [16] V. Beermann, M. Gocyla, E. Willinger, S. Rudi, M. Heggen, R. E. Dunin-Borkowski, M.-G. Willinger, P. Strasser, *Nano Lett.* **2016**, *16*, 1719.
- [17] C. Cui, L. Gan, H.-H. Li, S.-H. Yu, M. Heggen, P. Strasser, *Nano Lett.* **2012**, *12*, 5885.
- [18] C. Cui, L. Gan, M. Heggen, S. Rudi, P. Strasser, *Nat. Mater.* **2013**, *12*, 765.
- [19] X. Tuiev, S. Rudi, V. Petkov, A. Hoell, P. Strasser, *ACS Nano* **2013**, *7*, 5666.
- [20] E. Negro, A. Bach Delpuch, K. Vezzù, S. Polizzi, F. Bertasi, G. Nawn, G. Pagot, V. Di Noto, *ECS Trans.* **2016**, *72*, 1.
- [21] S. Wang, L. Xiong, J. Bi, X. Zhang, G. Yang, S. Yang, *ACS Appl. Mater. Interfaces* **2018**, *10*, 27009.
- [22] A. Oh, H. Baik, D. S. Choi, J. Y. Cheon, B. Kim, H. Kim, S. J. Kwon, S. H. Joo, Y. Jung, K. Lee, *ACS Nano* **2015**, *9*, 2856.
- [23] Q. Chang, Y. Xu, Z. Duan, F. Xiao, F. Fu, Y. Hong, J. Kim, S.-I. Choi, D. Su, M. Shao, *Nano Lett.* **2017**, *17*, 3926.
- [24] L. Gan, C. Cui, M. Heggen, F. Dionigi, S. Rudi, P. Strasser, *Science* **2014**, *346*, 1502.
- [25] M. Shviro, M. Gocyla, R. Schierholz, H. Tempel, H. Kungl, R. Eichel, R. E. Dunin-Borkowski, *Nanoscale* **2018**, *10*, 21353.
- [26] K. E. MacArthur, M. Heggen, R. E. Dunin-Borkowski, *Adv. Struct. Chem. Imaging* **2018**, *4*, 2.
- [27] L.-L. Wang, D. D. Johnson, *J. Am. Chem. Soc.* **2009**, *131*, 14023.
- [28] H. Kwon, M. K. Kabiraz, J. Park, A. Oh, H. Baik, S.-I. Choi, K. Lee, *Nano Lett.* **2018**, *18*, 2930.
- [29] Z. Niu, N. Becknell, Y. Yu, D. Kim, C. Chen, N. Kornienko, G. A. Somorjai, P. Yang, *Nat. Mater.* **2016**, *15*, 1188.
- [30] N. Becknell, Y. Son, D. Kim, D. Li, Y. Yu, Z. Niu, T. Lei, B. T. Sneed, K. L. More, N. M. Markovic, V. R. Stamenkovic, P. Yang, *J. Am. Chem. Soc.* **2017**, *139*, 11678.
- [31] Y. Xia, X. Xia, H.-C. Peng, *J. Am. Chem. Soc.* **2015**, *137*, 7947.
- [32] W. A. Al-Saidi, H. Feng, K. A. Fichtorn, *Nano Lett.* **2012**, *12*, 997.
- [33] M. Shviro, S. Polani, D. Zitoun, *Nanoscale* **2015**, *7*, 13521.
- [34] A. Thust, J. Barthel, K. Tillmann, *J. Large-Scale Res. Facil.* **2016**, *2*, A41.
- [35] A. Kovács, R. Schierholz, K. Tillmann, *J. Large-Scale Res. Facil.* **2016**, *2*, A43.